Solar Energy Materials & Solar Cells 211 (2020) 110550

Contents lists available at ScienceDirect

Solar Energy Materials and Solar Cells

journal homepage: http://www.elsevier.com/locate/solmat

The impact of interstitial Fe contamination on n-type Cz-Silicon for high efficiency solar cells

Ali Hajjiah [a,*], Marton Soha [b], Ivan Gordon [c], Jozef Poortmans [c], Joachim John [c]

[a] Kuwait University, College of Engineering and Petroleum, Electrical Engineering Department, Safat, Kuwait
[b] Debrecen University, Debrecen, Hungary
[c] IMEC (partner in EnergyVille), Kapeldreef 75, Leuven, Belgium

ARTICLE INFO

Keywords:
n-type Si Solar cell
High efficiency
Interstitial Fe Contamination
Effective minority carrier lifetime
QUOKKA simulations

ABSTRACT

In this work, we have investigated the impact of interstitial Fe contamination on the effective minority carrier lifetime of n-type Cz silicon bulk material for high efficiency solar cells. The study covers a Fe concentration in the silicon bulk from 3.5×10^{12} cm^{-3} to 2.7×10^{14} cm^{-3}. We have added 5 different concentrations (30, 100, 300, 1000 and 3000 ppb) of Fe intentionally to a wet chemical process tank and measured the transfer to the silicon wafer surface mimicking a possible contamination during wet chemical processing. In order to fabricate carrier lifetime test vehicles, the silicon wafer is then passivated with thermal silicon oxide from both sides. The surface contamination is driven into the bulk by mimicking a high temperature process during solar cell manufacturing. Effective minority carrier lifetime is measured at injection levels from 1×10^{13} cm^{-3} to 3×10^{15} cm^{-3}. We have fitted the theoretical curve for interstitial Fe derived from the SRH theory to the measured values and extracted the Fe contamination concentration. This value is comparable to the calculated value extracted from the surface contamination measurement. For low level injection (LLI), we extracted the capture cross section for interstitial Fe to be 6.45×10^{-17} cm/s $\pm$ 2.23×10^{-17} cm/s. The measured Fe contamination levels are used for the conversion efficiency fitting of a n-type bifacial silicon solar cell using QUOKKA simulations. The simulations show that very low Fe contamination concentrations of $[Fe]_{bulk} = 3.5 \times 10^{12}$ cm^{-3} ($[Fe]_{surf} = 6 \times 10^{10}$ cm^{-2}) already degrade the solar cell efficiency by 10% relative.

1. Introduction

Iron contamination can severely degrade the electrical performance of silicon solar cells [1]. The contamination can originate in Silicon solidified from lower-grade feedstock or in an inevitably impure crucible [2,3]. Gettering processes, like Phosphorous doping, are known to reduce the detrimental impact of this contamination during solar cell processing [4]. Feedstock manufacturing for mono-crystalline substrates using the Czochralski (Cz) method typically do not contain intrinsic iron in levels that are significant enough to impact the device performance. However, such substrates are severely impacted by extrinsic sources of iron contamination that can be present at many steps of the solar cell manufacturing process. As a result, degradation of the bulk lifetime can have a negative impact especially in higher efficiency cell architectures, in which the suppression of surface recombination by advanced passivation schemes leads to a strong dependence of efficiency on bulk lifetime.

In recent years the photovoltaic community has seen significant improvements in the efficiency of industrially produced solar cells as well as in the record efficiencies of elaborate lab-type cells [5–7]. This is due to improvements in surface passivation and process developments to utilize the high electrical quality of today's silicon wafers [8,9]. This high quality has been achieved by optimized process routes that deactivate recombination-active bulk defects in commercially available material [10–12]. Metallic impurities are common in photovoltaic grade crystalline silicon. Neutron activation analysis [13,14] studies of directionally solidified silicon have revealed significant quantities of Fe, Cr, Cu, Mo, and Co. These contaminants are especially damaging when occurring at interstitial or substitutional lattice sites.

Iron is a very common element in machine building and is difficult to eliminate on a production line. As a result, the unintentional iron contamination level in wafers is usually higher than that of other metal impurities [15]. The typical concentration of iron [Fe] in commercial multi-crystalline silicon ingots has been reported to be in the range of

* Corresponding author.
E-mail address: dr.hajjiah@gmail.com (A. Hajjiah).

https://doi.org/10.1016/j.solmat.2020.110550
Received 17 November 2019; Received in revised form 28 March 2020; Accepted 30 March 2020
Available online 9 April 2020

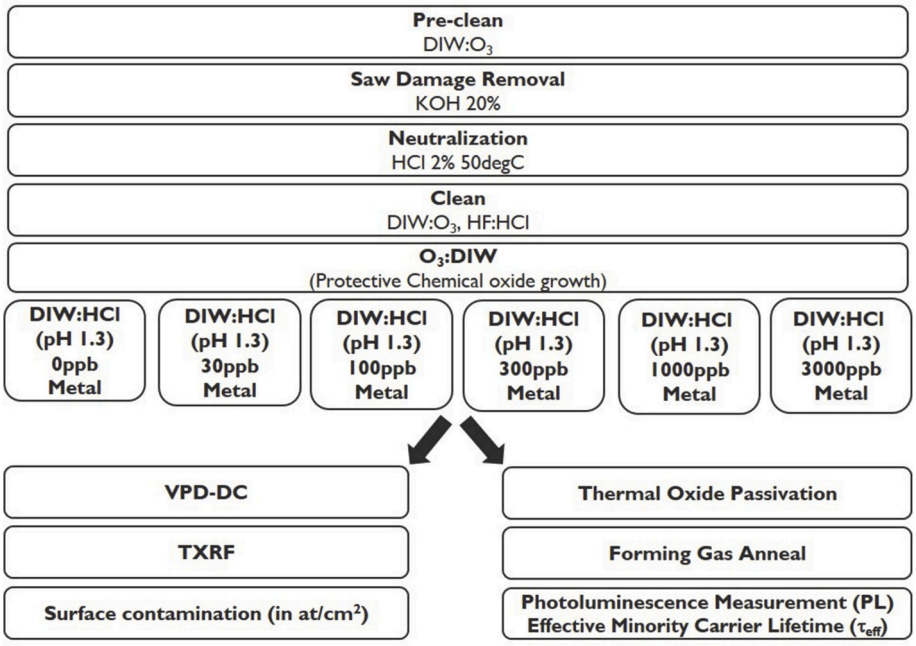

Fig. 1. A schematic representation with experimental splits of the process flow to investigate the effect of Fe contamination on bulk lifetime. Five wafers/split were used in this process.

10^{13}–10^{15} cm^{-3} as determined by neutron activation analysis (NAA) [16–19]. Iron can occur during crystal growth or wafer processing by either mechanical contact or liquid phase contact with iron-contaminated solutions. Once incorporated into a device, iron remains in either precipitated or dissolved form [20]. The precipitated iron in silicon contributes to increased leakage currents and reduced breakdown resistance, which causes degradation in device performance. Iron dissolved on interstitial lattice sites of silicon is electrically active and affects recombination in silicon and reduces the performance of solar cells. The major reasons why transition metals in general, and iron in particular, are detrimental for silicon devices are: (i) transition metals as well as their complexes and precipitates introduce deep levels in the band gap, reducing the minority carrier lifetime, or generating minority carriers in depleted regions; (ii) very high diffusion coefficients at high processing temperature ($D = 2.6 \times 10^{-6}$ cm^2/s at 1000 °C for Fe, [21]) can result in fast contamination of large wafer volumes even from point sources and from the wafer backside [22]. Numerous experimental data, obtained on intentionally and unintentionally iron-contaminated samples, suggested that dissolved Fe in silicon exhibits a donor level $Fe_i^{+/0}$ in the lower half of the band gap [$E_T \approx E_v + (0.38 \pm 0.05)$ eV] [23–33]. It took almost 20 years of research starting from the pioneering work of Collins and Carlson [34] to prove that this level is indeed the level of interstitial iron. Feichtinger provided experimental evidence that, within the limits from $E_C - 0.045$ eV to $E_V + 0.045$ eV, interstitial iron exists in only two charge states: Fe_i^0 and Fe_i^+ [35].

In this paper, we focus on the impact of interstitial iron in bulk concentrations between 3.45×10^{12} cm^{-3} to 2.77×10^{14} cm^{-3} on the effective minority carrier lifetime of n-type Cz-silicon material used for solar cell processing. The measured lifetime curves are fitted to the SRH theory taking one interstitial Fe impurity level at $E_t = 0.38$eV into account. The extracted impurity concentration is compared with the measured Fe surface concentration. In addition, we have extracted capture cross sections of the intrinsic Fe impurity from the slope of the lifetime curves at low level injection for different impurity levels. Finally, we have used the extracted data (impurity concentration and impurity energy level) to simulate conversion efficiencies for contaminated n-type silicon solar cells using the QUOKKA simulation tool.

2. Experimental approach and study logic

2.1. Experimental approach

The wafers used for the experiment were commercially available n-type large-area (156×156 mm^2) semi-square Cz-Silicon material (3–5 Ω cm resistivity and 180–200 um thickness).

The preparation of the samples includes a pre-clean for organic contamination removal, a saw damage etch in concentrated KOH to obtain a damage free, smooth surface and subsequent neutralization. The metal clean was done using a clean based on DIW:O_3 + HF:HCl mixtures as described by Haslinger et al. [36]. The clean was followed by an extra de-ionized water DIW:O_3 treatment to create a clean chemical oxide and therefore have a stable hydrophilic surface.

The contamination bath is a 13l quartz beaker that is cleaned overnight in HNO_3 based chemistry, rinsed in DIW until a resistivity of >5MOhm. The holders are also cleaned in this solution and rinsed in DIW. The wafers were then immersed in a Fe-contaminated acidic solution[1] for 5min and received a subsequent DIW overflow rinse for 5min and N_2 spin drying. No feed and bleed dosing is applied. The chemicals are stirred during mixing but not during the 5 min contamination process. After this contamination process, a part of the wafers were measured using the combined method of VPD-DC (Vapor Phase Decomposition – Droplet Collection) and TXRF (Total Reflection X-Ray Fluorescence) as described by Hellin et al. [37], on another part of the wafers a thermal oxidation process was conducted (975 °C for 1 h), providing 20 nm SiO_2 for surface passivation followed by an annealing under forming gas (5%H_2 in N_2) at 450 °C for 3 h. A schematic drawing for the detailed process flow can be found in Fig. 1.

To measure the effective lifetime (τ_{eff}), quasi-steady-state photoconductance (QSSPC) [38] measurements were conducted using a BT Imaging tool on a symmetric lifetime test vehicle where the effective surface recombination velocity at both the front side and the rear side of

[1] The solution is a diluted HCl:DIW mixture (pH 1.3) spiked with ICP-Standard solution at 1000 ppm to obtain Fe concentration of 30, 100, 300, 1000 and 3000 ppb. A reference test is also done without any Fe contamination added (0 ppb).

the sample can be assumed equal and close to zero due to thermal oxide passivation on both surfaces, i.e. $S_{eff\text{-}front} = S_{eff\text{-}rear} = S_{eff} = 0$. The symmetric structure is then used to extract effective lifetime (τ_{eff}) using the Kane and Swanson approach [39].

In order to study the impact of surface contamination in the range as low as 1e10 cm^{-2}, n-type cz-silicon material of high minority carrier lifetime has been used. The minority carrier lifetime of the non-contaminated material was determined to be well above 4 ms at 1e15 cm^{-3}.

2.2. Study logic

Here, we describe the study logic of our investigation in a step by step approach:

Step 1. Intentionally controlled contamination of the acidic cleaning solution with Fe, mimicking a processing tank that has been loaded with metal impurities during solar cell manufacturing. Outcome: measured Fe concentration $[Fe]_{liq}$ in the liquid in ppb

Step 2. Quantifying the metal transfer from the solution to the wafer surface by measuring the surface concentration of the added metal impurity by VDP-DC-TXRF. Outcome: measured Fe concentration $[Fe]_{surf}$ on the wafer surface in cm^{-2}

Step 3. Applying a high temperature process step, like thermal oxidation, to diffuse the metal impurities from the surface into the bulk of the silicon wafer. Effective minority carrier lifetime is determined from the achieved symmetric test vehicles. The lifetime values of the contaminated samples are subtracted from the lifetime values of the non-contaminated sample to extract the lifetime degradation coming from the Fe impurity only (τ_{Fe}). The extracted impurity surface concentration from Step 2 is used to calculate the impurity bulk concentration assuming all the surface impurities are diffused into the bulk. This Fe impurity concentration value is called $[Fe]_{bulk\_calc}$. Outcome: calculated bulk iron impurity concentration $[Fe]_{bulk\_calc}$ in cm^{-3} and measured τ_{eff}. τ_{Fe} is calculated from τ_{eff}.

Step 4. At low injection (dn « n0), the linear part of the iron contaminated minority carrier lifetime curve is fitted to the SRH minority carrier lifetime model, to extract the capture cross section of the Fe impurity. Here we assume that all the Fe species from the surface are diffused into the bulk and are electrically active. Outcome: capture cross section σ_p of the Fe impurity by fitting

Step 5. The injection independent part of the Fe contaminated lifetime curves is fitted to the SRH minority carrier lifetime model to determine the Fe impurity concentration. Here we use the extracted capture cross section from Step 4. This Fe impurity concentration value is call $[Fe]_{bulk\_fit}$. Outcome: Bulk iron impurity concentration $[Fe]_{bulk\_fit}$ in cm^{-3} by fitting

Step 6. Comparing the Fe bulk concentration values achieved from the two different approaches. If the values coincide, we can conclude that all the iron of the surface has diffused into the bulk and became electrically active and that the lifetime degradation we measure in n-type Cz-silicon is related to interstitial iron in the silicon bulk.

Step 7. The achieved capture cross section and Fe bulk concentrations are used in the QUOKKA device simulator to predict solar cell efficiencies depending on metal impurity level.

3. Theoretical background

3.1. Deriving the Shockley-Read-Hall lifetime limit for a single defect trap level

In the contamination process, control wafers without Fe contamination were co-processed. The effective carrier lifetimes τ_{eff} for both contaminated ($\tau_{diffused}$) and control wafers without Fe diffusion ($\tau_{control}$) were measured in the same injection level range. Therefore, the carrier lifetime only due to the introduced Fe_i (τ_{Fe}) can be extracted using Eq. (1) [40]

$$\frac{1}{\tau_{Fe}} = \frac{1}{\tau_{diffused}} - \frac{1}{\tau_{control}} \tag{1}$$

This procedure subtracts out the influence of other recombination effects such as Auger and surface recombination. Also, to correlate between the bulk and the surface concentration, Eq. (2) is used, if all the Fe species on the surface are diffused into the bulk after a thermal oxidation treatment.

$$[Fe]_{bulk\_calc} = \frac{2 \times [Fe]_{surface}}{W} \tag{2}$$

In the above equation, W is the thickness of the wafer, $[Fe]_{surf}$ is the amount of Fe impurities injected in the solution and measured at the surface of the wafer, and $[Fe]_{bulk}$ is the amount of Fe impurities expected in the bulk of the wafer after the thermal diffusion process.

Based on the Shockley–Read–Hall theory (SRH theory) of carrier generation and recombination at a single defect level with energy E_t, the SRH lifetime (i.e. $\Delta n = \Delta p$) can be expressed as:

$$\tau_{SRH} = \frac{\tau_{no}(p_1 + p_o + \Delta n) + \tau_{po}(n_1 + n_o + \Delta n)}{p_o + n_o + \Delta n} \tag{3}$$

where τ_{no} and τ_{po} are the capture time constants, Δn is the excess carrier density from injection, n_o and p_o are the equilibrium densities of electrons and holes respectively, and finally, p_1 and n_1 are the carrier densities which are defined in Eq. (4) and Eq. (5) as

$$n_1 = N_c exp\left(\frac{-E_c - E_t}{kT}\right) \tag{4}$$

$$p_1 = N_v exp\left(\frac{-E_t - E_v}{kT}\right) \tag{5}$$

Here N_c and N_v are the effective densities of states in the conduction and the valence bands respectively, E_t is the energy level of the recombination center, E_c is the conduction band energy, while E_v is the energy in the valence band.

In the limit of low-level injection (LLI: Δn « $n_o + p_o$), the SRH lifetime, Eq. (3), for a n-type ($n_o \gg p_o$) semiconductor can be written as shown in Eq. (6)

$$\tau_{SRH}^{LLI,n} = \tau_{po}\left[\left(1 + \frac{n_1}{n_o}\right) + \left(\frac{p_1}{n_o}\right)\right] \tag{6}$$

$Fe_i^{+/0}$ impurities in n-type Silicon are most effective for recombination because they are deep defects with energy levels close to the mid-bandgap. In such defects, the minority capture time constant is the limiting process over a large injection level range [41]. Hence, the resulting low-level injection SRH lifetime is independent of doping concentration and equal to the minority capture time constant [i.e. $\tau_{SRH}^{LLI,n} \approx \tau_{po}$]. However, in the limit of high-level injection (HLI: $\Delta n \gg n_o + p_o, n_1, p_1$), the SRH lifetime becomes independent of both the doping concentration and the injection level and is only limited by the slower of the two capture processes (i.e. $\tau_{SRH}^{HLI,n} = \tau_{po}$ *for n − type semiconductor*).

If the SRH lifetime is injection independent

$$\left(\text{i.e.}\Delta\tau_{SRH} = \tau_{SRH}^{HLI,n} - \tau_{SRH}^{LLI,n} = 0\right),$$

τ_{SRH} will simplify to:

$$\tau_{SRH} = \tau_{po} = \left(N_t \sigma_p v_{th}\right)^{-1} \tag{7}$$

with.

Table 1
Fe concentration in the acidic cleaning solutions in ppb and in mol/L.

Concentration in ppb	30	100	300	1000	3000
Concentration in mol/L	5.79×10^{-7}	1.79×10^{-6}	5.79×10^{-6}	1.79×10^{-5}	5.79×10^{-5}

Table 2
Summary of the values for interstitial Fe concentration and capture cross section. The errors are determined from the best-fit of the measured data to the model equations. For the values extracted by the TXRF measurement in column 2 we assume a 10% error margin.

$[Fe]_{liq}$ [ppb]	$[Fe]_{surf}$ [cm^{-2}]	$[Fe]_{bulk\_calc}$ [cm^{-3}]	$\sigma_p(Fe_i)_{\_fit}$ [cm/s]	$[Fe]_{bulk\_fit}$ [cm^{-3}]
[Fe] in ppb concentration added as intentionally controlled contamination	$[Fe]_{surf}$ measured surface concentration in cm^{-2}	$[Fe]_{bulk\_calc}$ = Nt from $[Fe]_{surf}$ calculated bulk concentration in cm^{-3}	capture cross section extracted from the fitted model in cm/s	$[Fe]_{bulk\_fit}$ = Nt bulk concentration extracted from the fitted model in cm^{-3}
30	**$6.11 \cdot 10^{10}$**	**4.50E + 12**	**8.06E-17 ± 2.38E-17**	**3.45E + 12 ± 0.96E + 12**
100	**$1.00 \cdot 10^{11}$**	**4.03E + 13**	**5.13E-17 ± 1.69E-17**	**4.30E13 ± 1.41E13**
300	**$2.73 \cdot 10^{11}$**	**1.13E + 14**	**6.89E-17 ± 0.83E-17**	**9.85E13 ± 1.18E13**
1000	**$1.34 \cdot 10^{12}$**	**1.68E + 14**	**5.04E-17 ± 0.86E-17**	**1.94E14 ± 0.33E14**
3000	**$3.14 \cdot 10^{12}$**	**2.26E + 14**	**4.55E-17 ± 0.23E-17**	**2.77E14 ± 0.14E14**

$N_t = [Fe_i]$ in cm^{-3} (impurity concentration in the bulk)
$\sigma_p = 4.54 \times 10^{16}$ (-0.05 × T/k_B) cm^{-2} (capture cross section)
$v_{th} = 1.1 \times 10^7$ cm/s (thermal velocity)

3.2. Deriving the capture cross section for interstitial Fe

The capture cross section can be extracted by fitting the t_{eff} at low level injection (LLI: $\Delta n \ll n_o$) with the linear function:

$$\tau_{SRH} = \frac{\tau_{no}(p_1 + p_o) + \tau_{po}(n_1 + n_o)}{n_o} + \frac{\tau_{no}}{n_o}\Delta n = b + m\Delta n \quad (8)$$

For n-type silicon the capture cross section for interstitial Fe can be extracted following B. Paudyal et al. [42].

$$\sigma_p = \left(N_t \tau_{po} v_{th}\right)^{-1} = \left(slope \times n_o v_{th} N_t\right)^{-1} \quad (9)$$

with $n_0 = 9 \times 10^{14}$ cm^{-3} (n-type Cz-silicon background doping level).

4. Results and discussion

In this chapter the results of the experiments described in the study logic plan are presented.

4.1. Step 1 And 2: intentionally contaminated process bath and metal impurity determination at the wafer surface

From the five Fe contamination levels C_{liq} (see Table 1) we have intentionally added to the cleaning solution (Step 1), we could measure the resulting Fe surface concentrations transferred to the silicon wafer surface with VPC-DC-TXRF (Step 2). The surface concentrations $[Fe]_{surf}$ are shown in the 2nd column of Table 2.

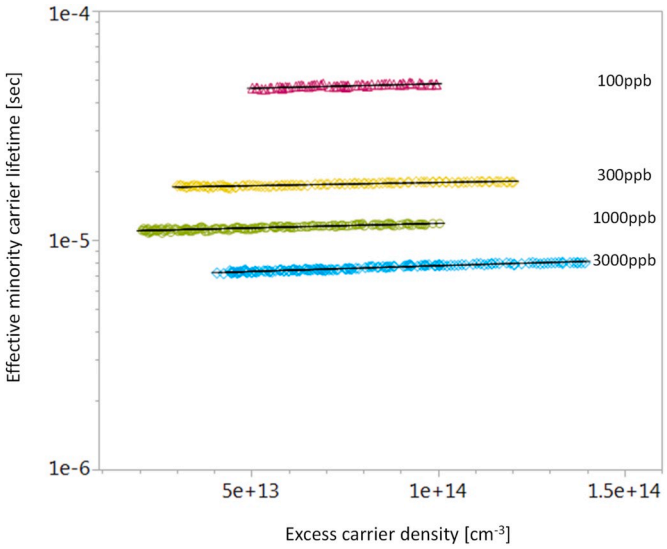

Fig. 2. Effective minority carrier lifetime vs excess carrier density at low level injection (LLI) for the liquid contamination concentrations in the range 100–3000 ppb. From the slope of the fitted curves the capture cross section is extracted.

4.2. Step 3: Calculating the metal impurity concentration in the silicon bulk material after a high temperature process step

From these values the diffused bulk concentrations are calculated using eq. (2), assuming that all the Fe is diffused from the surface into the bulk after the high temperature process of thermal oxidation (Step 3). The resulting bulk concentrations $[Fe]_{bulk\_calc}$ are listed in the 3rd column of Table 2.

4.3. Step 4: Extracting the capture cross section from the slope of the minority carrier lifetime curve

Fig. 2 shows the Fe contaminated lifetime values (Step 3) and the theoretical fit at low level injection (LLI) over an excess carrier density range from 1×10^{13} cm^{-3} to 1.5×10^{14} cm^{-3}. We have chosen 4 lifetime value sets (100 ppb, 300 ppb, 1000 ppb and 3000 ppb) to extract the slope and calculate the capture cross section following equations (8) and (9). The lifetime curve for 30 ppb in LLI is not depicted because of a limited amount of data points. Nevertheless, we could extract the capture cross section also from this lifetime curve but with increased error margin. The capture cross section of interstitial iron varies in literature depending on the applied measurement method. The capture cross section values $s_p(Fe_i)_{\_fit}$ (at room temperature) extracted from the slope of the iron contaminated minority carrier lifetime curve at LLI are depicted in the 4th column of Table 2. The extracted capture cross section values compare well with the literature values for interstitial Fe which are varying between 3×10^{-17} cm/s [43] and 14×10^{-17} cm/s [44] at room temperature.

4.4. Step 5: Extracting the metal impurity concentration from minority carrier lifetime curves

The measured effective minority carrier lifetime vs injection level per contamination level has been fitted with eq. (7) over an excess carrier density range from 1×10^{14} to 3×10^{15} cm^{-3}, depicted in Fig. 3. The impurity concentration in the bulk (N_t) extracted from this fit gives the Fe concentration and type of the Fe impurity (Step 5). We could fit the

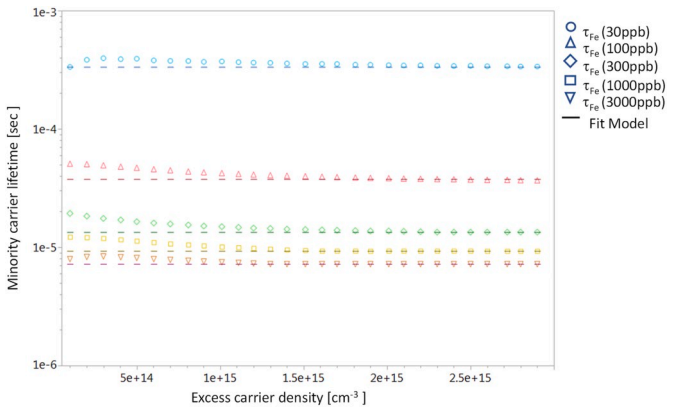

Fig. 3. Fe contaminated minority carrier lifetime level vs excess carrier concentration.

lifetime values with the assumption that there is a single trap of interstitial iron. The resulting Fe concentrations $[Fe]_{bulk\_fit}$ are shown in the 5th column of Table 2. The errors are determined from the best-fit of the measured data to the model equations.

4.5. *Step 6: Comparing the bulk Fe concentrations calculated from the surface and from the fit model*

The Fe concentration in the silicon bulk is determined using two different methods (see steps 3 and 5). In Table 3 we compare the results of the two methods and give the deviation. The deviation of the two methods is in the range of 10–20% depending on the contamination concentration. Taking this relatively small deviation into account we can conclude that the fit model is valid, and the minority carrier lifetime of the silicon wafer can be described by the SRH theory assuming a single trap of interstitial Fe.

4.6. *Step 7: Introducing the achieved results into the QUOKKA device simulator*

The Quokka device simulator [45] provides a feature to determine conversion efficiency of silicon solar cells with increased SRH generation and recombination due to metal contamination. For this the following parameters need to be introduced in the simulation tool: name of the metal impurity, interband trap energy E_t, impurity concentration N_t, capture cross section s.

Fig. 4 depicts a Quokka simulation of a n-type bifacial PERT silicon solar cell with a measured efficiency of 22% [46]. The degradation of the efficiency as a function of Fe contamination is simulated using the extracted values (N_t and σ_p) for interstitial Fe_i (E_t = 0.38 eV). As a comparison, literature values [47] extracted by SENTAURUS DEVICE simulation software is depicted, simulating the impact of interstitial Fe contamination on a n-type PERC cell with 21.4% non-contaminated efficiency. Both simulations show the expected similar behaviour. A 10% relative reduction in efficiency is expected with a Fe impurity concentration of 3×10^{12} at/cm^3 in the bulk. For Fe concentrations above 10^{14} at/cm^3 the expected efficiency loss is more that 6% absolute.

5. Conclusion

The presented intentionally controlled contamination approach delivers a reproducible procedure for investigation of metal impurities in silicon bulk material for impurity levels from 3.5×10^{12} to 2.75×10^{14} cm^{-3} [48].

Fe bulk concentration is determined applying two different methods. The fact that both independent methods provide the same results, supports the assumption that all the Fe atoms originally present at the surface have been driven into the bulk and become electrically active as interstitial Fe after a thermal oxidation at 975 °C for 1 h.

The capture cross section for interstitial iron in n-type silicon is extracted by fitting the slope of the Fe contaminated lifetime curve at low level injection. This method provides capture cross section values of 6.45×10^{-17} cm/s ± 2.23×10^{-17}cm/s. This value is consistent to published literature values varying from 3×10^{-17} to 14×10^{-17} cm/s.

QUOKKA device simulations have been executed using the extracted values for iron bulk concentrations and capture cross section. The simulated values for a bifacial n-type silicon solar cell with a starting, non-contaminated, conversion efficiency of 22% are showing the detrimental impact of the Fe contamination on the solar cell efficiency. A contamination level of $[Fe]_{bulk} = 3.5 \times 10^{12}$ cm^{-3} ($[Fe]_{surf} = 6 \times 10^{10}$cm^{-2}) degrades the solar cell by 10% relative.

Declaration of competing interest

As Ivan Gordon, a co-author on this paper, is the Editor-in-Chief of Solar Energy Materials and Solar Cells, he was blinded to this paper during review and the paper was independently handled by Simon Philipps.

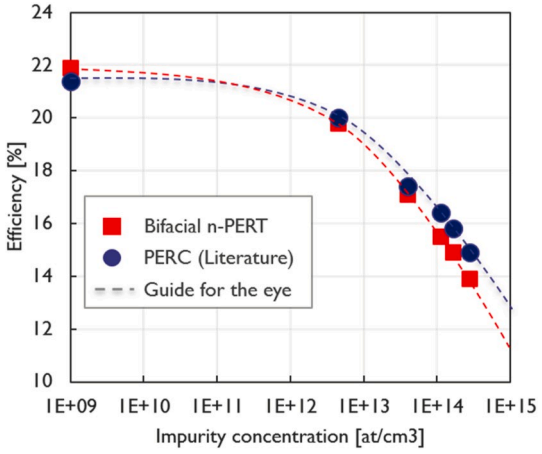

Fig. 4. The input parameter for the device simulation are the interstitial Fe trap energy level (E_t = 0.38 eV), the impurity concentration in the silicon bulk material [Fe_i] and the capture cross section. (For interpretation of the references to colour in this figure legend, the reader is referred to the Web version of this article.)

Table 3
Comparison of the Fe concentration in the silicon bulk determined with two different methods.

	30 ppb	100 ppb	300 ppb	1000 ppb	3000 ppb
[Fe] in cm^{-3} calculated from the surface concentration	4.50E+12 ± 0.45E+12	4.03E+13 ± 0.40E+13	1.13E+14 ± 0.11E+14	1.68E+14 ± 0.17E+14	2.26E+14 ± 0.23E+14
[Fe] in cm^{-3} extracted from the fit to the lifetime curve	3.45E+12 ± 0.96E+12	4.30E+13 ± 1.41E+13	9.85E+13 ± 1.18E+13	1.94E+14 ± 0.33E+14	2.77E14 ± 0.28E14
Mean Deviation	1.05E+12	1.2E+12	1.45e+13	2.6E+13	5.1E+13

CRediT authorship contribution statement

Ali Hajjiah: Conceptualization, Formal analysis, Writing - original draft, Writing - review & editing, Supervision. **Marton Soha:** Conceptualization. **Ivan Gordon:** Formal analysis, Writing - review & editing. **Jozef Poortmans:** Supervision. **Joachim John:** Conceptualization, Formal analysis, Writing - original draft, Writing - review & editing, Supervision.

Acknowledgement

The authors acknowledge the financial support of their partners in IMEC's industrial affiliation program (IIAP). The work in this paper was partially funded by the Kuwait Foundation for the Advancement of Sciences under project number CN18-15EE-01. Imec is a partner in EnergyVille (www.energyville.be), a collaboration between the Flemish research partners KU Leuven, VITO, imec, and UHasselt in the field of sustainable energy and intelligent energy systems.

Appendix A. Supplementary data

Supplementary data to this article can be found online at https://doi.org/10.1016/j.solmat.2020.110550.

Appendix

Determination of the solubility of interstitial iron

The achieved values for capture cross section are compared with literature data for interstitial Fe in n-type silicon and the Fe concentration is compared with the amount measured at the surface. The extracted values can be explained by assuming a single impurity state of interstitial Fe using the SRH theory.

In order to check the physical constrains of our findings, we have calculated the solubility of Fe in the applied experimental set up. Graff [20] gives an empirical equation for the solubility of Fe_i in crystalline silicon

$$S = 5 \times 10^{22} \times \exp(8.2 - 2.94/kT)$$

Using our process temperature of 980 °C (1253 K), we calculate kT = 0.1081 eV. Which provides a solubility of

$$S = 2.8 \times 10^{14}\ cm^{-3}$$

Our highest value for Fe concentration is calculated to be $2.77 \times 10^{14}\ cm^{-3}$. Hence, with our highest contamination level we are just under the solubility limit of interstitial Fe, i.e. in this work we are still under the limit to form Fe precipitates.

The result also shows the limited influence of oxide precipitates on the effective minority carrier lifetime.

Parameters

Table 4
Parameters used in simulations

Parameter	Value	
n_i	9.95E9	cm^{-3}
$n_o = N_d$	1E15	cm^{-3}
$p_o = N_a = ni^2/N_d$	99.0025E3	cm^{-3}
E_g	1.12	eV
E_t-E_v	0.39	eV
E_c-E_t	0.73	eV
N_c	2.82E19	cm^{-3}
N_v	1.83E19	cm^{-3}
V_{th}	1E7	eV
Boltzmann constant (k)	8.62E-5	$eV.K^{-1}$
n_1	15508962.97	cm^{-3}
p_1	5.16139E12	cm^{-3}

References

[1] D. Macdonald, A. Cuevas, "Reduced fill factors in multicrystalline silicon solar cells due to injection-level dependent bulk recombination lifetimes, Prog. Photovoltaics 8 (4) (2000) 363–375.
[2] G. Coletti, "Sensitivity of state-of-the-art and high efficiency crystalline silicon solar cells to metal impurities, Prog. Photovoltaics 21 (5) (2013) 1163–1170.
[3] G. Coletti, R. Kvande, V.D. Mihailetchi, L.J. Geerligs, L. Arnberg, E.J. Øvrelid, Effect of iron in silicon feedstock on p- and n-type multicrystalline silicon solar cells, J. Appl. Phys. 104 (10) (2008).
[4] M. Kivambe, D.M. Powell, S. Castellanos, M.A. Jensen, A.E. Morishige, K. Nakajima, K. Morishita, R. Murai, T. Buonassisi, Minority-carrier lifetime and defect content of n-type silicon grown by the noncontact crucible method, J. Cryst. Growth 407 (2014) 31–36.
[5] F. Fertig, R. Lantzsch, A. Mohr, M. Schaper, M. Bartzsch, D. Wissen, F. Kersten, A. Mette, S. Peters, A. Eidner, J. Cieslak, K. Duncker, M. Junghänel, E. Jarzembowksi, M. Kauert, B. Faulwetter-Quandt, D. Meißner, B. Reiche, S. Geißler, S. Hörnlein, C. Klenke, L. Niebergall, A. Schönmann, A. Weihrauch, F. Stenzel, A. Hofmann, T. Rudolph, A. Schwabedissen, M. Gundermann, M. Fischer, J.W. Müller, D.J.W. Jeong, Mass production of p-type Cz silicon solar cells approaching average stable conversion efficiencies of 22 %, Energy Procedia 124 (2017) 338–345.
[6] K. Yoshikawa, H. Kawasaki, W. Yoshida, T. Irie, K. Konishi, K. Nakano, T. Uto, D. Adachi, M. Kanematsu, H. Uzu, K. Yamamoto, Silicon heterojunction solar cell with interdigitated back contacts for a photoconversion efficiency over 26%, Nat. Energy 2 (5) (2017) 17032.
[7] M.A. Green, Y. Hishikawa, E.D. Dunlop, D.H. Levi, J. Hohl-Ebinger, A.W.Y. Ho-Baillie, Solar cell efficiency tables (version 37), Prog. Photovoltaics Res. Appl. 26 (1) (2018) 3–12.

[8] J. John (Ed.), Surface Passivation of Industrial Crystalline Silicon Solar Cells, IET publishing, London, 2018.
[9] J. John, S. Jambaldinni, M. Haslinger, M. Gocyla, A. Hajjiah, I. Kuzma-Filipek, L. Tous, R. Russell, F. Duerinckx, J. Szlufcik, J. Poortmans, The impact of advanced texturing on saturation current density in n-type PERT silicon solar cell processing, in: Proceedings of 35th European Photovoltaic Solar Energy Conference and Exhibition, EUPVSEC, Brussels, Belgium, 2018.
[10] A. Herguth, G. Hahn, Kinetics of the boron-oxygen related defect in theory and experiment, J. Appl. Phys. 108 (11) (2010), 114509.
[11] P. Hamer, B. Hallam, S. Wenham, M. Abbott, Manipulation of hydrogen charge states for passivation of P-type wafers in photovoltaics, IEEE J. Photovolt. 4 (5) (2014) 1252–1260.
[12] M.B. Shabani, T. Yamashita, E. Morita, Study of gettering mechanisms in silicon: competitive gettering between phosphorus diffusion gettering and other gettering sites, Solid State Phenom. 131–133 (2008) 399–404.
[13] A.A. Istratov, T. Buonassisi, R.J. McDonald, A.R. Smith, R. Schindler, J.A. Rand, J. P. Kalejs, E.R. Weber, Metal content of multicrystalline silicon for solar cells and its impact on minority carrier diffusion length, J. Appl. Phys. 94 (2003) 6552.
[14] D. Macdonald, A. Cuevas, A. Kinomura, Y. Nakano, "Proceedings of the 29th Photovoltaic Specialists Conference New Orleans," LA, IEEE, New York, 2002, p. 285.
[15] L. Jastrzebski, J. Lagowski, W. Henley, P. Edelman, in: D.C. Jacobson, D.E. Luzzi, T.F. Heinz, M. Iwaki (Eds.), In Beam-Solid Interactions for Materials Synthesis and Characterization, Mater. Res. Soc., Pittsburgh, 1995, p. 405.
[16] A.A. Istratov, T. Buonassisi, R.J. McDonald, A.R. Smith, R. Schindler, J.A. Rand, J. P. Kalejs, E.R. Weber, J. Appl. Phys. 94 (2003) 6552.
[17] D. Macdonald, A. Cuevas, A. Kinomura, Y. Nakano, L.J. Geerligs, J. Appl. Phys. 97 (2005), 033523.
[18] A.A. Istratov, H. Hieslmair, E.R. Weber, Appl. Phys. Mater. Sci. Process A70 (2000) 489.
[19] C.C. Swanson, A.J. Filo, J.P. Lavine, J. Radioanal. Nucl. Chem. 248 (2001) 69.
[20] K. Graff, Metal Impurities in Silicon-Device Fabrication, Second ed., vol. 24, Springer, Berlin, 1999.
[21] E.R. Weber, Appl. Phys. A A30 (1983) 1.
[22] W. Bergholz, G. Zoth, F. Gelsdorf, B. Kolbesen, in: W.M. Bullis, U. Gösele (Eds.), Defects in Silicon II, The Electrochem. Soc., Pennington, 1991, p. 21.
[23] J.D. Gerson, L.J. Cheng, J.W. Corbett, J. Appl. Phys. 48 (1977) 4821.
[24] K. Nakashima, Jpn. J. Appl. Phys. 24 (1985) 1018.
[25] Y. Kamiura, M. Yoneta, F. Hashimoto, Phys. Status Solidi 120 (1990) K11.
[26] N.H. Sheng, J.L. Merz, J. Appl. Phys. 55 (1984) 3083.
[27] J.T. Borenstein, J.T. Jones, J.W. Corbett, G.S. Oehrlein, R.L. Kleinhenz, Appl. Phys. Lett. 49 (1986) 199.
[28] M.L. Swanson, Phys. Status Solidi 33 (1969) 721.
[29] H. Indusekhar, V. Kumar, Phys. Status Solidi 95 (1986) 269.
[30] N.I. Akulovich, V.V. Petrov, V.D. Tkachev, Sov. Phys. Semiconduct. 16 (1982) 969.
[31] H. Feichtinger, A. Gschwandtner, J. Waltl, Phys. Status Solidi 53 (1979) K71.
[32] W. Leskoschek, H. Feichtinger, G. Vidrich, Phys. Status Solidi 20 (1973) 601.
[33] N.H. Sheng, J.L. Merz, Physica 116B (1983) 553.
[34] C.B. Collins, R.O. Carlson, Phys. Rev. 108 (1957) 1409.
[35] H. Feichtinger, J. Waltl, A. Gschwandtner, Solid State Commun. 27 (1978) 867.
[36] M. Haslinger, M. Soha, S. Jambaldinni, A. Hajjiah, J. Szlufcik, J. Poortmans, J. John, Novel wet chemical cleaning concepts for high efficiency silicon solar cells, in: Proceedings of the 33rd European Photovoltaic Solar Energy Conference and Exhibition - EUPVSEC, 2017, pp. 628–630.
[37] D. Hellin, J. Rip, S. Arnauts, S. De Gendt, P.W. Mertens, C. Vinckier, Spectrochim. Acta B Atom Spectrosc. 59 (8) (2004) 1149–1157.
[38] R.A. Sinton, A. Cuevas, Appl. Phys. Lett. 69 (17) (1996) 2510.
[39] D.E. Kane, R.M. Swanson, Measurement of the emitter saturation current by a contactless photoconductivity decay method, in: Proceedings of the 18th IEEE Photovoltaic Specialists Conference, New York, IEEE, 1985, pp. 578–583.
[40] D. Macdonald, L.J. Geerligs, Appl. Phys. Lett. 85 (No. 18) (1 November 2004).
[41] S. Rein, T. Rehrl, W. Warta, S.W. Glunz, J. Appl. Phys. 91 (No. 4) (15 February 2002).
[42] B.B. Paudyal, K.R. McIntosh, D.H. Macdonald, in: Photovoltaic Specialists Conference (PVSC), 2009 34th IEEE, IEEE, 2009. S. 001588-001593.
[43] K. Wunstel, P. Wagner, Interstitial iron and iron-acceptor pairs in silicon, Appl. Phys. A 27 (1982) 207.
[44] H. lndusekhar, V. Kumar, Properties of iron related quenched-in levels in p-silicon, Phys. Status Solidi 95 (1986) 269–278.
[45] A. Fell, A free and fast 3D/2D solar cell simulator featuring conductive boundary and quasi-neutrality approximations, IEEE Trans. Electron. Dev. 60 (2) (2012) 733–738.
[46] J. Chen, L. Tous, S. Singh, P. Choulat, F. Duerinckx, J. Szlufcik, "Screenprinted large area rear-junction n-PERT solar cells with efficiencies above 22.0% and bifaciality ~ 90%," Presentation at 12th SNEC (2018) International Photovoltaic Power Generation and Smart Energy Exhibition & Conference.
[47] J. Schmidt, B. Lim, D. Walter, K. Bothe, S. Gatz, T. Dullweber, P. Andermatt, Impurity-related limitations of next-generation industrial silicon solar cells, IEEE J. Photovoltaics 3 (No. 1) (2013).
[48] J. John, A. Hajjiah, M. Haslinger, M. Soha, A. Uruena, E. Cornagliotti, L. Tous, P. Mertens, J. Poortmans, Solar energy materials and solar cells 194 (1 June 2019) 83–88.